White-light emitting ZnO–$SiO_2$ nanocomposite thin films prepared by the target-attached sputtering method



2006 Nanotechnology 17 174

(http://iopscience.iop.org/0957-4484/17/1/028)

INSTITUTE OF PHYSICS PUBLISHING NANOTECHNOLOGY
Nanotechnology **17** (2006) 174–180 doi:10.1088/0957-4484/17/1/028

# White-light emitting ZnO–$SiO_2$ nanocomposite thin films prepared by the target-attached sputtering method

**Yu-Yun Peng**[1], **Tsung-Eong Hsieh**[1] **and Chia-Hung Hsu**[2]

[1] Department of Materials Science and Engineering, National Chiao-Tung University, 1001 Ta-Hsueh Road, Hsinchu, Taiwan 300, Republic of China
[2] Research Division, National Synchrotron Radiation Research Center, 101 Hsin-Ann Road, Hsinchu Science Park, Hsinchu, Taiwan 300, Republic of China

E-mail: pyy.mse90g@nctu.edu.tw, tehsieh@cc.nctu.edu.tw and chsu@nsrrc.org.tw

Received 21 June 2005, in final form 6 October 2005
Published 1 December 2005
Online at stacks.iop.org/Nano/17/174

**Abstract**
ZnO–$SiO_2$ nanocomposite thin films were prepared using the target-attached RF sputtering method without substrate heating. The PL measurements showed that the $SiO_2$ films containing uniformly dispersed ZnO nanoparticles emit white light consisting of violet, blue, and green–yellow band emissions. The presence of the blue emission is attributed to the large number of ZnO/$SiO_2$ interfaces, which enlarges the depletion layer width and then enhances the related transition. The Gaussian curve fitting of PL spectra revealed that the competition between the blue and green–yellow band emissions and the relative emission intensity is strongly associated with the number of ZnO nanoparticles embedded in the $SiO_2$ matrix. XPS analysis revealed that the main component of the oxygen defect species in the ZnO nanocomposite thin films is '$O^-$' ions (531.1–531.7 eV) at the subsurface. Within the knowledge of the defect configuration, XPS data were also utilized to estimate the oxygen vacancies and the specific carrier concentration in ZnO nanoparticles and relate to the integrated intensities of emission bands. Further analyses indicated that the defect structure of samples could be manipulated by the number and distribution of ZnO nanoparticles in $SiO_2$ matrix to yield a distinct luminescence spectrum.

(Some figures in this article are in colour only in the electronic version)

## 1. Introduction

Zinc oxide (ZnO) is a wide-bandgap semiconductor ($E_g$ = 3.25–3.5 eV) with many desirable physical properties. In addition to emission in the UV region, ZnO also emits a broad luminescence emission in the green–yellow region. Its large exciton binding energy (59 meV) gives rise to high efficiency exciton emission at room temperature. These properties render it a potential material for blue- or white-light emitting devices [1]. Many studies reported that nano-sized ZnO exhibits a unique luminescence property different from that of the bulk ZnO [2–4]. Because nanoparticles possess an enormous surface-to-volume ratio, the interaction between ZnO nanoparticles and surrounding materials can strongly affect the emission spectrum and thus offers an effective means to engineer its optoelectronic properties. Therefore, ZnO-based nanocomposites have attracted much attention in recent years. Several methods such as sol–gel [5], molecular capping [6], and impregnation [7] have been employed to disperse ZnO nanoparticles in silica or polymeric matrices. In this work, white-light emitting ZnO–$SiO_2$ nanocomposite thin films are prepared using the target-attached RF co-sputtering without substrate heating. The emission property and the microstructure of the samples so obtained are presented.

## 2. Experimental details

High purity ZnO chips were placed on a 3″ quartz target during RF sputtering to fabricate ZnO–$SiO_2$ nanocomposite

**Table 1.** The ZnO content of ZnO–$SiO_2$ nanocomposite thin films. The binding energies of the Zn 2p levels and the three kinds of oxygens obtained from the XPS curve fitting analysis are also listed.

| | | Binding energy (eV) | | | | |
|---|---|---|---|---|---|---|
| Sample | ZnO (at.%) | Zn $2p_{1/2}$ | Zn $2p_{3/2}$ | $O_{lattice}$ | $O^-$ ion | $O^{2-}$ ion |
| a | 3.67 | 1045.20 | 1022.25 | 530.507 | 531.762 | 532.521 |
| b | 7.42 | 1045.15 | 1022.30 | 530.453 | 531.684 | 532.613 |
| c | 11.39 | 1045.20 | 1022.25 | 530.401 | 531.701 | 532.550 |
| d | 15.49 | 1045.05 | 1022.15 | 530.239 | 531.443 | 532.194 |
| e | 18.40 | 1045.20 | 1022.10 | 530.330 | 531.380 | 532.209 |
| f | 26.36 | 1045.30 | 1022.20 | 530.281 | 531.179 | 532.069 |
| g | 39.74 | 1045.05 | 1022.10 | 530.409 | 531.312 | 532.351 |
| h | 45.03 | 1045.10 | 1022.15 | 530.412 | 531.526 | 533.145 |

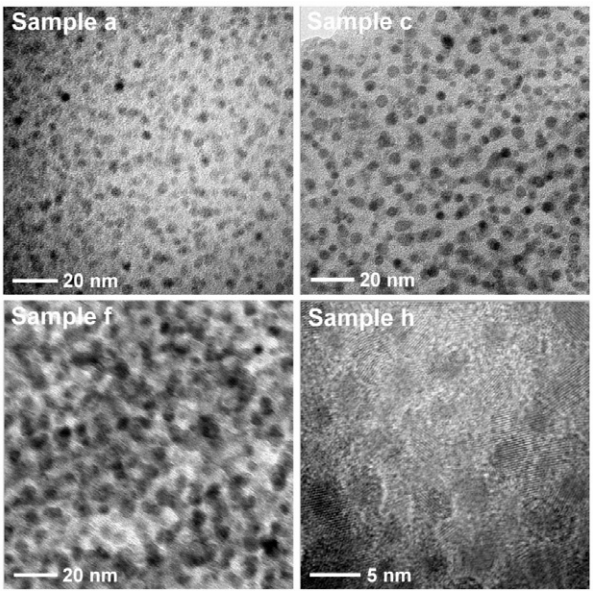


**Figure 1.** The TEM micrographs of samples a, c, f, and h. Nano-sized ZnO particles (dark points) are randomly dispersed within the amorphous $SiO_2$ matrix (light regions).

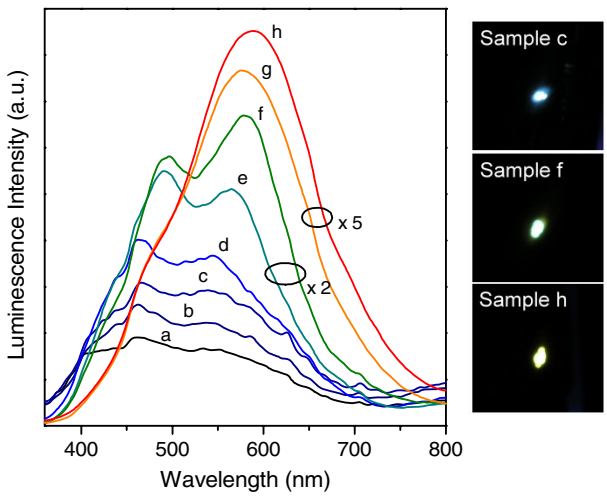


**Figure 2.** The PL spectra of ZnO–$SiO_2$ nanocomposite thin films. The right-hand panels show the colour of light exiting from PL measurement for samples c, f and h.

thin films. The number of chips was adjusted to control the ZnO content. Sputtering proceeded with 100 W RF power at 5 mTorr Ar pressure and the base pressure of the growth chamber is a few times $10^{-7}$ Torr. Si wafers are used as substrates and all the deposited layers are approximately 140 nm thick. It is noteworthy that no substrate heating upon deposition or post-growth annealing was carried out. The microstructure of the samples was characterized by x-ray diffraction (XRD, MacScience M18XHF-SRA, with $\lambda = 0.154$ nm) and transmission electron microscopy (TEM, Philips TECNAI 20). The composition was examined by x-ray photoemission spectroscopy (XPS) with a Mg K$\alpha$ source (American Physical Electronics ESCA PHI 1600). The PL spectra were measured at room temperature using a 325 nm He–Cd laser.

## 3. Results and discussion

### *3.1. Composition and microstructure of the ZnO–Si $O_2$ nanocomposites*

XPS was performed to characterize the composition of the samples. No peak associated with metallic Zn and bulk Si was identified and both Zn and Si were in the oxidized states. Therefore, we define the ZnO content as the atomic ratio of Zn to the sum of Zn and Si, i.e. Zn/(Zn + Si). Obtained ZnO content, as listed in table 1, exhibits a monotonic increase with increasing chip-to-target ratio. Figure 1 displays the TEM micrographs of the ZnO–$SiO_2$ nanocomposite samples. It can be readily seen that ZnO forms nanoparticles of diameter 3–6 nm embedded in the amorphous $SiO_2$ matrix. With increasing chip-to-target ratio, from samples a to h, number density of the ZnO nanoparticles increases. For samples g and h, the overlapping and coalescence of nanoparticles becomes severe, while the well resolved lattice planes in high magnification images indicates the good crystallinity of the ZnO nanoparticles. The crystal structure of the ZnO nano-crystallites was examined by XRD in grazing incidence geometry and is confirmed to be wurtzite. The average size of the nanoparticles estimated from the width of the (110) diffraction peak following the Scherrer equation is 4.5 ± 0.5 nm, in good agreement with the TEM observation. We further analysed the size distribution of the nanoparticles from the TEM images. For each micrograph, the diameters of over 50 nanoparticles were measured and their size distribution was modelled by a Gaussian function. The average diameter and full width at half maximum (FWHM) of size distribution are depicted by the filled squares and error bars in figure 9 as a

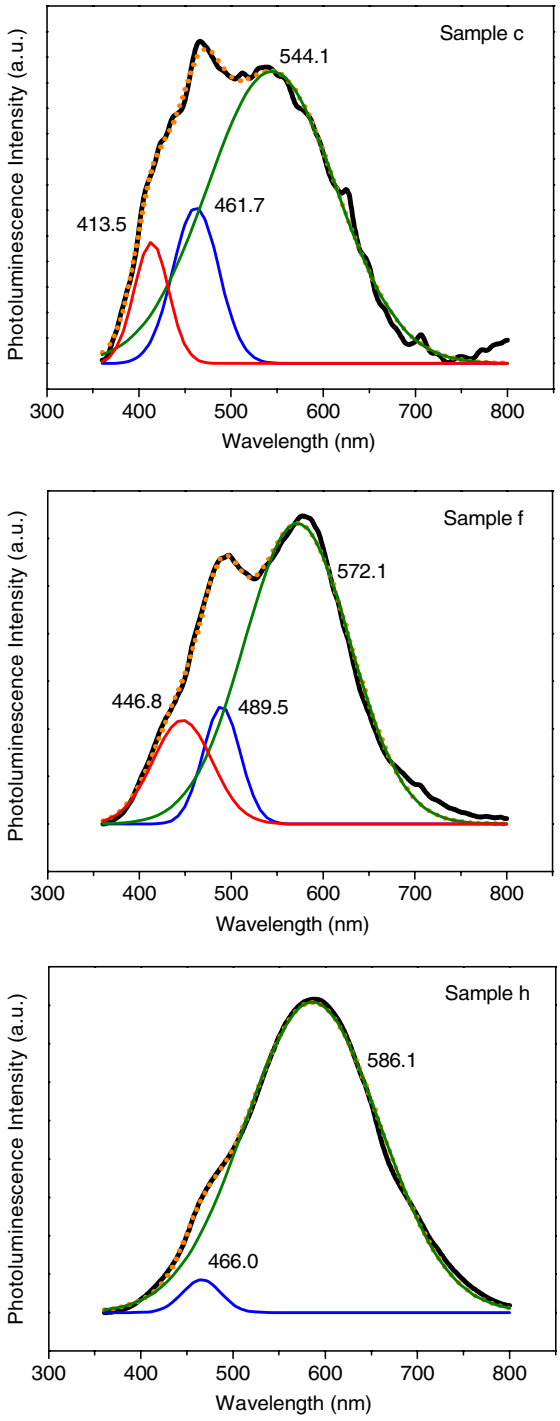


**Figure 3.** The Gaussian curve fitting of PL spectra of samples c, f and h.

function of ZnO content. In spite of the large dispersion in size, the average particle diameter does show a trend of slight growth with increasing ZnO content up to ∼26 at.%. For the samples of the highest ZnO contents, i.e. g and h, the observed coalescence of the particles makes visual differentiation of one particle from the other rather difficult and leads to a large uncertainty in size determination. Moreover, in some regions the lattice planes of the neighbouring particles looks aligned with each other, indicative of the formation of aggregates of ZnO nanoparticles at high ZnO contents.

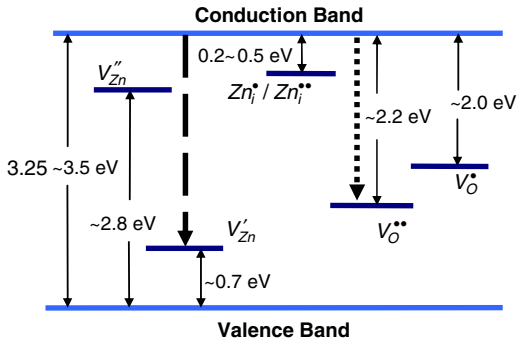


**Figure 4.** The schematic defect energy levels of ZnO. The dotted arrow line indicates the green–yellow emission transition from CB to deep trap $V_O^{\bullet\bullet}$, and the dashed arrow line indicates the blue emission transition from CB to $V'_{Zn}$.

### *3.2. Photoluminescence and the Gaussian fittings*

Figure 2 illustrates the PL spectra of the ZnO–$SiO_2$ films together with three photographs, displayed on the right panel, showing the colour of emitted lights out of three samples of different ZnO content. White-light emission was observed for samples with low ZnO content (samples a–d). As the ZnO content increases, the emitted light gradually becomes yellow and the profile of the emission spectra changes as well. The spectra are analysed by Gaussian curve fitting as shown in figure 3 and the obtained fitting parameters are summarized in table 2. The fitting results revealed that the spectra consist of three bands located in violet, blue, and green–yellow regions, respectively. For samples with the low ZnO content, the spectra have the luminescence intensity maxima in the blue band region. However, the spectra of samples with high ZnO content, samples g and h, exhibit a nearly symmetric broad band dominated by the yellow emission. It should be noticed that, as the ZnO content increases, the intensity of the green–yellow band grows enormously with the diminishing of the blue band.

### *3.3. Emission mechanisms*

Figure 4 schematically shows the defect energy levels of ZnO. Among the visible emissions of ZnO [2, 3, 8–12], the green–yellow emission of the ZnO particles is attributed to the radiative recombination of electrons from the conduction band (CB) edge and deeply trapped holes ($V_O^{\bullet\bullet}$) in the bulk of the ZnO particles [3]. The recombination centre $V_O^{\bullet\bullet}$ (green, 2.2 eV) is formed as a result of $V_O^{\bullet} \rightarrow V_O^{\bullet\bullet}$ transition ($V_O^{\bullet}$, dominant defect ∼2.0 eV below CB) promoted by the hole trapping of $O_i''$ at the ZnO surface. It is speculated that the embedding of ZnO nanoparticles into the $SiO_2$ matrix generates an $O_i''/O_i'$-rich interfacial region and thus promotes the $V_O^{\bullet} \rightarrow V_O^{\bullet\bullet}$ transition and the green–yellow emission.

Figure 5 plots the peak intensity ratio of the blue emission to green–yellow emission versus the ZnO at.%. Hence, the blue emission cannot come from the blue shift of the green–yellow band due to the quantum confinement effect; its origin should be different from that of the green–yellow emission and most probably related to the microstructure. One reason for this argument is that the blue emission is frequently observed

**Table 2.** The results of Gaussian curve fitting of PL spectra of ZnO–$SiO_2$ nanocomposite thin films. The obtained parameters include peak position, band width and the integrated area ratio of blue emission to green–yellow emission (unit nm).

| | Violet band | | Blue band | | Green–yellow band | | |
|---|---|---|---|---|---|---|---|
| Sample | Peak 1 | Width | Peak 2 | Width | Peak 3 | Width | Integration area ratio of peak 2 to peak 3 |
| a | 405.5 | 37.1 | 457.2 | 60.5 | 547.9 | 133.0 | 0.3555 |
| b | 410.8 | 36.4 | 458.4 | 50.5 | 540.6 | 136.8 | 0.2616 |
| c | 413.5 | 37.6 | 461.7 | 49.8 | 544.1 | 139.0 | 0.1912 |
| d | 416.6 | 33.6 | 459.1 | 46.1 | 539.2 | 143.9 | 0.1768 |
| e | 438.0 | 53.9 | 485.0 | 40.6 | 554.7 | 122.1 | 0.1628 |
| f | 446.8 | 64.9 | 489.5 | 40.8 | 572.1 | 114.7 | 0.1388 |
| g | — | — | 469.0 | 41.5 | 577.7 | 142.0 | 0.0385 |
| h | — | — | 466.0 | 40.8 | 586.1 | 146.5 | 0.0297 |

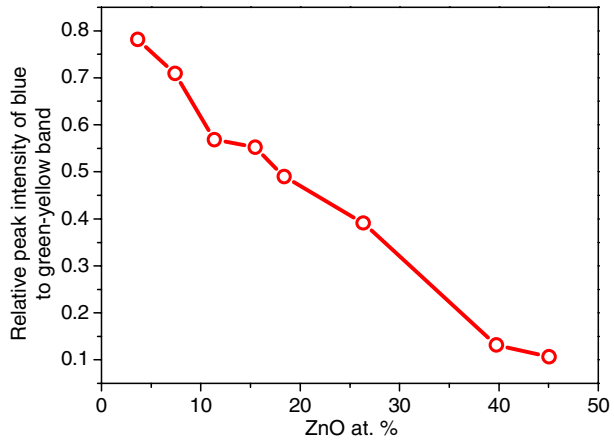


**Figure 5.** The peak intensity ratio of blue emission to green–yellow emission versus the ZnO at.%.

in the composite systems [5, 11, 12, 14–16] but less seen in pure ZnO thin films or powders with grains of $\mu$m or even only 100 nm [2, 9, 13]. These observations indicate that the blue emission is strongly related to the heterogeneous boundaries, not ZnO/ZnO interfaces. The other reason is that the special feature of the band bending occurred in ZnO grains gives rise to the thought of correlating the blue emission with the depletion region. The band bending at particle surfaces creates an electron depletion region of width $W$ which is inversely proportional to the intensity of the green–yellow emission [2, 9]. According to this, we infer that sample a possesses the maximum $W$ while sample h possesses the minimum $W$. However, the relative intensity of blue emission to green–yellow emission has a maximum in sample a and a minimum in sample h, which evidences that the blue emission originates from the depletion region. The defect level responsible for the blue emission can thus be assigned to $V'_{Zn}$, which is about 0.7 eV above the valence band and exists only in the depletion region [9, 10].

Previous studies attributed violet emission to the donor–acceptor pair with the longitudinal optical (LO-) phonon replicas [1, 3, 9, 17–19]. However, with the data available, we are not certain about the mechanism responsible for the violet emission (∼405 nm, 3.06 eV) and will not discuss it further here.

### *3.4. XPS analysis*

To obtain the chemical states of different elements within the samples, we performed detailed analysis on XPS spectra. Figures 6(a) and (b) depict the XPS spectra of Zn 2p and O 1s, respectively. In all samples, the binding energies of Zn $2p_{1/2}$ (1045.20 ± 0.10 eV) and Zn $2p_{3/2}$ (1022.20 ± 0.10 eV) are both slightly larger than the values of Zn in the bulk ZnO. This indicates that Zn is in the formal $Zn^{2+}$ valence state within an oxygen deficient $ZnO_{1-x}$ environment [20].

Dupin *et al* proposed that, there exist various oxygen ionizations associated with the weakly adsorbed species in many oxide systems and they could be resolved by analysing the profile of O 1s XPS spectra [21]. In the case of ZnO, there exist two different oxygen species: lattice oxygen $O_{lattice}$, termed as '$O^{2-}$', in the crystalline network (530.1–530.4 eV), and '$O^{-}$' ions, with sites where the coordination number of oxygen ions is smaller than that in regular sites, e.g. subsurface (531.2–531.7 eV). In addition to the two oxygen species in ZnO mentioned above, there exists another one in the ZnO–$SiO_2$ system, denoted as '$O^{2-}$' (∼532.4 eV), which is attributed to the loosely bound oxygen in the amorphous $SiO_2$ or partially weakly adsorbed oxygen species such as $OH^-$ or $CO_3^{2-}$. The shift of the O 1s peak position from ∼532.3 eV toward lower binding energy to ∼531 eV, as shown in figure 6(b), reflects the decrease of the relative amount of $O^{2-}$ as compared with $O_{lattice}$ and $O^-$ when the ZnO content increases. As to a quantitative description of the growth/diminishing of each component, detailed analysis is required.

The O 1s peaks of the XPS curves were decomposed using the curve fitting program XPSPEAK 4.1 with a combination of Gaussian (80%) and Lorentzian (20%) distributions. Figure 7 illustrates the curve fitting result of sample h. The fitted results of XPS data are listed in table 1. From the curve fittings, we observed excess '$O^{-}$' ions existing in all samples generated during the sputtering as reported by Chen *et al* [22], which consists of the luminescences promoted by an $O''_i/O'_i$-rich environment. The XPS data were further utilized for the calculations of carrier concentration and depletion width presented below.

### *3.5. Specific carrier concentration and the depletion width*

The relative amount of $O_{lattice}$ could be calculated from the integrated area of the corresponding peak relative to the total integrated area of the O 1s peak. Together with the atomic percentage given by XPS data, the atomic ratio of $O_{lattice}$

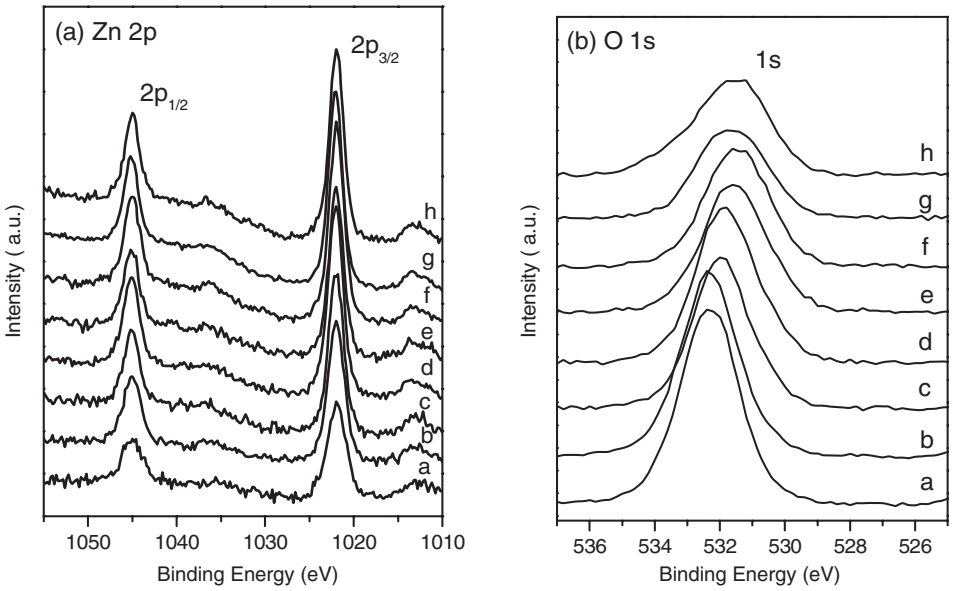


**Figure 6.** XPS data of (a) Zn 2p peaks and (b) O 1s peak of the ZnO–$SiO_2$ nanocomposite thin films.

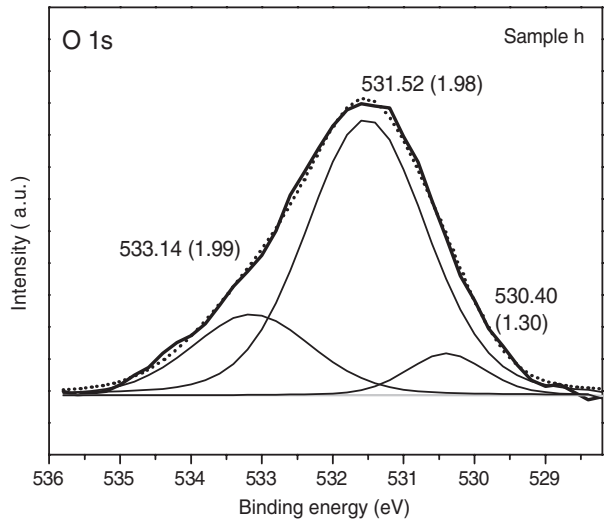


**Figure 7.** O 1s peak of sample h is fitted by a combination of Gaussian (80%) and Lorentzian (20%) distributions. The value inside the brackets is the corresponding FWHM.

to Zn is decided. Based on the argument that the $V_O^{\bullet}$ state is the dominant oxygen vacancy in ZnO, not $V_O^{\bullet\bullet}$ [23–26], together with the reaction of $V_O^{\times} \rightarrow V_O^{\bullet} + e'$ and the ratio of $O_{lattice}$ to Zn, we calculate $[V_O^{\bullet}]$ and use it as the specific donor concentration, $N_d$, in the ZnO nanoparticles. In our calculation, we ignored the contribution of '$O^-$' species, which may lead to an overestimate of the specific carrier density since '$O^-$' ions may grab electrons and reduce the free carriers inside the ZnO nanoparticles. However, the error of the overestimation should be less than one order because $O_i'$ is not the dominating defect species in the lattice in general.

The depletion width $W$ of nanoparticles is then calculated according to the equation $W = \sqrt{2\varepsilon_{ZnO}V_{bi}/eN_d}$, where $V_{bi}$ stands for the potential at the boundary, $e$ is the electron charge, $N_d$ is the specific donor density, and $\varepsilon_{ZnO}$ denotes the static dielectric constant of ZnO. In the calculation, we have $\varepsilon_{ZnO} = 8.85\varepsilon_0$ and $V_{bi} = 0.15$ eV, which is estimated from $N_d$ according to the simplest 1D solution for the Poisson's equation [27]. The obtained specific donor concentration and the calculated depletion width are listed in table 3.

**Table 3.** The estimated atomic ratio of lattice O to Zn, the specific carrier concentration $N_d$, the depletion width $W$, and the specific volume ratio $V_{depletion}/V_{bulk}$.

| Sample | $O_{lattice}$:Zn | $N_d$ ($cm^{-3}$) | $W$ (Å) | $V_{depletion}/V_{bulk}$ |
|---|---|---|---|---|
| a | 0.946 | $2.23 \times 10^{21}$ | 2.505 | 0.427 |
| b | 0.871 | $5.35 \times 10^{21}$ | 1.623 | 0.252 |
| c | 0.809 | $7.96 \times 10^{21}$ | 1.332 | 0.201 |
| d | 0.796 | $8.50 \times 10^{21}$ | 1.288 | 0.194 |
| e | 0.742 | $1.07 \times 10^{22}$ | 1.146 | 0.170 |
| f | 0.672 | $1.36 \times 10^{22}$ | 1.017 | 0.149 |
| g | 0.533 | $1.95 \times 10^{22}$ | 0.851 | 0.123 |
| h | 0.484 | $2.15 \times 10^{22}$ | 0.810 | 0.116 |

As mentioned earlier, we attributed the origin of the blue and green–yellow emissions to the depletion and the bulk regions, respectively. Therefore, the specific volume ratio of depletion to bulk regions of ZnO nanoparticles should be proportional to the ratio of total carrier number bound to the corresponding emissions, which is equivalent to the ratio of the integrated intensity of the blue band to the green–yellow band in PL spectra. Figure 8 plots the estimated specific volume ratio of the depletion region to the bulk and the calculated carrier number ratio with respect to the ZnO at.%. The two curves follow each other very well; the consistency supports the models of the green–yellow and blue emission mechanisms proposed above. The discrepancy observed in samples g and h may result from the PL curve fittings, in which the blue band almost submerges in the tail of the dominant green–yellow band. Under this circumstance, the huge intensity difference may introduce significant uncertainty in determining the peak

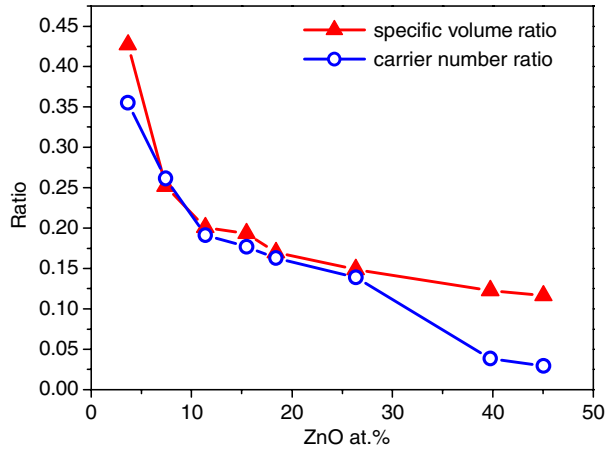


**Figure 8.** The relationship of the specific volume ratio ($V_{depletion}/V_{bulk}$) and the carrier number ratio of blue to green–yellow emission (integration area ratio of peak 2 to peak 3) with the ZnO at.%.

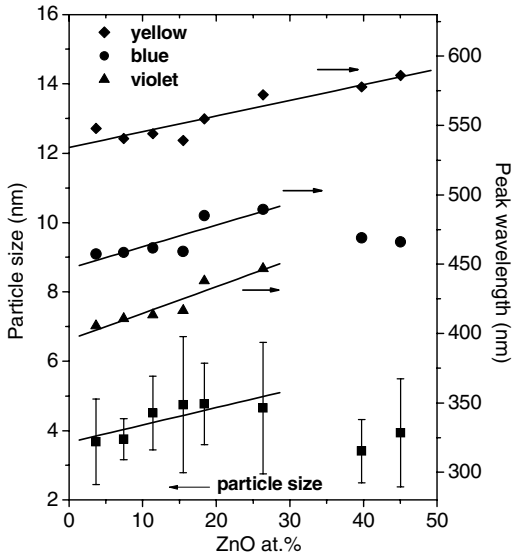


**Figure 9.** The variation of the particle size and the peak wavelength of each emission band with ZnO at.%.

position and the integrated area. Although we ascribe the blue emission to the trap level $V'_{Zn}$, the difference between $[V^{\bullet}_{O}]$ and $[V'_{Zn}]$ in the bulk and depletion regions, respectively, has not been clarified. Therefore, an additional cause of the discrepancy is that $[V'_{Zn}]$ may decrease dramatically when the depletion width is extremely small. The probability of the carrier recombination in the depletion region may also be reduced as well and cause the abrupt decay of the blue emission.

### *3.6. Quantum confinement effect on luminescences*

We plot the peak wavelength of the three visible emission bands in PL spectra and the ZnO particle size distribution as a function of ZnO content in figure 9. We found that all the emission bands shift to lower energy (about 0.15–0.3 eV) as ZnO content increases up to ∼26 at.%. Within the same range, the average particle size exhibits a slight growth with increasing ZnO content. This correlation suggests that the quantum confinement effect plays a role in governing the emission properties in these ZnO–$SiO_2$ nanocomposite films within low ZnO contents. Besides this, the separation distance between nanoparticles may also have some effect. Since ZnO nanoparticles are embedded in the $SiO_2$ matrix, a material with a huge bandgap, the separation distance may affect the effective potential barrier height and the coupling between the nanoparticles, and consequently the discrete energy levels [28–31]. For the samples with ZnO content over ∼30 at.%, the shift of the emission band and change of particle size do not follow the same trend as in the low ZnO content region in figure 9. This could be due to the large experimental uncertainty resulting from the very weak blue emission and coalescence of the nanoparticles mentioned earlier. In fact, the emission property of high ZnO content samples is very similar to that of bulk ZnO, which agrees with the observation of the formation of ZnO aggregates.

## 4. Conclusions

In conclusion, the ZnO–$SiO_2$ nanocomposite thin films exhibiting white-light emission consisting of the violet, blue, and green–yellow band emissions have been prepared using the target-attached RF sputtering method without substrate heating. The Gaussian curve fitting and defect structure analysis revealed that blue emission results from the transition of electrons at CB to trap level $V'_{Zn}$, and, the transition of electrons at CB to trap level $V^{\bullet\bullet}_{O}$ is responsible for the green–yellow band emission. The violet emission might be attributed to the donor–acceptor-pair with the longitudinal optical (LO)-phonon replicas. The change of relative intensity between the green–yellow and blue emissions is attributed to the variation of the depletion layer width and the free carrier concentration. This work not only demonstrates a novel method to prepare white-light emission ZnO–$SiO_2$ thin films, but also suggests that the defect structure and transition mechanisms of samples could be modified by the number and the distribution of ZnO nanoparticles in the $SiO_2$ matrix to yield the distinct luminescence property.

## Acknowledgments

This work is supported by the National Science Council (NSC) of the Republic of China under contract No NSC92-2216-E009-013. Y-YP would like to acknowledge the NSC for financial support under contract NSC93-2112-M-213-007.

## References

[1] Reynolds D C, Look D C, Jogai B and Morkoc H 1997 *Solid State Commun.* **101** 643
[2] Vanheusden K, Warren W L, Seager C H, Tallant D R and Voigt J A 1996 *J. Appl. Phys.* **79** 7983

[3] Dijken A V, Meulenkamp E A, Vanmaekelbergh D and Meijerink A 2000 *J. Lumin.* **87–89** 454
[4] Jing L, Xu Z, Shang J, Sun X, Cai W and Guo H 2002 *Mater. Sci. Eng.* A **332** 356
[5] He H, Wang Y and Zou Y 2003 *J. Phys. D: Appl. Phys* **36** 2972
[6] Guo L, Yang S, Yang C, Yu P, Wang J, Ge W and Wong G K L 2000 *Appl. Phys. Lett.* **76** 2901
[7] Cannas C, Mainas M, Musinu A and Piccaluga G 2003 *Compos. Sci. Technol.* **63** 1187
[8] Liu M, Kitai A H and Mascher P 1992 *J. Lumin.* **54** 35
[9] Wu X L, Siu G G, Fu C L and Ong H C 2001 *Appl. Phys. Lett.* **78** 2285
[10] Lima S A M, Sigoli F A, Jafelicci M Jr and Davolos M R 2001 *Int. J. Inorg. Mater.* **3** 749
[11] Abdullah M, Shibamoto S and Okuyama K 2004 *Opt. Mater.* **26** 95
[12] Abdullah M, Morimoto T and Okuyama K 2003 *Adv. Funct. Mater.* **13** 800
[13] Yuldashev S U, Panin G N, Choi S W, Yalishev V S, Nosova L A, Ryu M K, Lee S, Jang M S, Chung K S and Kang T W 2003 *Japan. J. Appl. Phys.* **42** 3333
[14] Yu Y S, Kim G Y, Min B H and Kim S C 2004 *J. Eur. Ceram. Soc.* **24** 1865
[15] Pal U, García-Serrano J, Casarrubias-Segura G, Koshizaki N, Sasaki T and Terahuchiy S 2004 *Sol. Energy Mater. Sol. Cells* **81** 339
[16] Pal U, García-Serrano J, Koshizaki N and Sasaki T 2004 *Mater. Sci. Eng.* B **113** 24
[17] van Dijken A, Makkinje J and Meijerink A 2001 *J. Lumin.* **92** 323
[18] Ong H C and Du G T 2004 *J. Cryst. Growth* **265** 471
[19] Teke A, Özgür Ü, Doğan S, Gu X, Morkoc H, Nemeth B, Nause J and Everitt H O 2004 *Phys. Rev.* B **70** 195207
[20] Major S, Kumar S, Bhatnagar M and Chopra K L 1986 *Appl. Phys. Lett.* **49** 394
[21] Dupin J C, Gonbeau D, Vinatier P and Levasseur A 2000 *Phys. Chem. Chem. Phys.* **2** 1319
[22] Chen M, Wang X, Yu Y H, Pei Z L, Asi X D, Sun C, Huang R F and Wen L S 2000 *Appl. Surf. Sci.* **158** 134
[23] Kröger F A 1974 *The Chemistry of Imperfect Crystals* vol 2 (Amsterdam: North-Holland) chapter 16
[24] Hagemark K I 1976 Defect structure of Zn-doped ZnO *J. Solid State Chem* **16** 293
[25] Sukker M H and Tuller H L 1983 Defect equilibria in ZnO varistor materials *Advances in Ceramics* vol 7 *Additives and Interfaces in Electric Ceramics* ed M F Yan and A H Heuer (OH: American Ceramic Society) p 71
[26] Han J, Mantas P Q and Senos A M T 2002 *J. Eur. Ceram. Soc.* **22** 49
[27] Srikant V and Clarke D R 1997 *J. Appl. Phys.* **81** 6357
[28] Mukherji D and Nag B R 1975 *Phys. Rev.* **12** 4338
[29] Bastard G 1981 *Phys. Rev.* B **24** 5693
[30] Chuang S L 1995 *Physics of Optoelectronic Devices* (New York: Wiley) chapter 4.7
[31] Bastard G 1988 *Wave Mechanics Applied to Semiconductor Heterostructures* (New York: Halsted)